2017-07

Deep UV hardening of photoresist for shaping of graphene and lift-off fabrication of back-gated field effect biosensors by ion-milling and sputter deposition

Li, B

10.1016/j.carbon.2017.03.032
Carbon
Elsevier BV

Carbon 118 (2017) 43–49

Contents lists available at ScienceDirect

Carbon

journal homepage: www.elsevier.com/locate/carbon

Deep UV hardening of photoresist for shaping of graphene and lift-off fabrication of back-gated field effect biosensors by ion-milling and sputter deposition

Bing Li [a, b, c, *], Genhua Pan [a], Ahmed Suhail [a], Kamrul Islam [a], Neil Avent [b], Paul Davey [a]

[a] Wolfson Nanomaterials & Devices Laboratory, Faculty of Science and Engineering, University of Plymouth, Plymouth, Devon, PL4 8AA, UK
[b] Centre for Research in Translational Biomedicine, Plymouth University Peninsula Schools of Medicine and Dentistry, University of Plymouth, Devon, PL4 8AA, UK
[c] Department of Physics, Faculty of Natural Sciences, Imperial College London, London, SW7 2AZ, UK

ARTICLE INFO

Article history:
Received 21 December 2016
Received in revised form
19 February 2017
Accepted 10 March 2017
Available online 14 March 2017

Keywords:
Graphene
Ion-milling shaping and lift-off fabrication
Immunosensor
Label-free detection

ABSTRACT

The development of microfabrication techniques compatible with scalable production processes of semiconductor industry is of crucial importance for the technological exploitation of graphene. We report here a novel technique for the photolithographic fabrication of back-gated field-effect transistor immunosensors using chemical vapor deposited (CVD) graphene. The CVD graphene was transferred following polymer assisted method and shaped by ion-milling rather than conventional oxygen plasma etching. A deep UV hardening technique was applied, respectively, before the ion milling shaping of graphene channels and before the deposition of Cr/Au layers for the lift-off fabrication of FET electrodes to ensure the removability of the photoresist. The quality of resulting graphene FET was confirmed by Raman spectroscopy, optical spectroscopy and the detection towards an ultralow concentration of human chorionic gonadotropin. SEM cross-sectional analysis revealed that the deep UV (DUV) hardening process prevents the formation of a post-etching residue shell at the high local temperature during the ion-milling process or sputtering deposition and hence maintain the integrity and significantly improve the removability of the photoresist without the need of using sonication. By using this ion-milling shaped and lift-off fabricated graphene immunosensor, a limit-of-detection of 6 pg/ml has been achieved with a detection range from 1 pg/ml to 100 ng/ml for the label-free detection of hCG.

1. Introduction

The unique chemical and physical properties of graphene, such as high electronic and thermal conductivity, 2D nature, intrinsically high surface to volume ratio and chemical inertness, have been believed to be capable of yielding biosensors with an extremely high sensitivity and also compatible with the current large-scale device fabrication processes [1]. Therefore, compared with the conventional biosensors, graphene-based biosensors have the potential to exhibit improved sensing performance with a lower commercial cost [2,3]. Among the graphene biosensors reported to date, field-effect transistors (FET) in the form of ion-gated structure has been reported in numerous studies since its first reported by Mohanty and Berry [4]. However, back-gated FETs possess a promising role for effective detection of multiple biomarkers on an array based system for diagnosing diseases that require simultaneous detection of different biomolecules facilitating scalable industrial production. The large-scale production of graphene on the transition metal foil provided the opportunity to design and fabricate graphene-based electronic devices with a reproducible geometric dimension. Prior to our work, the scalable shaping of graphene was normally achieved by oxygen plasma etching [5,6]. Some other techniques, such as focused ion beam (FIB) etching [7,8], photo-catalytic shaping [9] and reactive-ion etching (RIE), have also been reported. For the direct shaping of graphene using FIB etching, the geometry of graphene design can be precisely controlled due to the size of the focused beam. However, the removal of carbon atoms using this technique is incomplete and the shaping efficiency is too low to meet the requirement of large-scale industrial production [10]. For the photo-catalytic shaping of

* Corresponding author. Current address: Department of Physics, Faculty of Natural Sciences, Imperial College London, London, SW7 2AZ, UK.
E-mail address: b.li@imperial.ac.uk (B. Li).

http://dx.doi.org/10.1016/j.carbon.2017.03.032

graphene, although the photo-generated, highly reactive ·OH radicals could be used as sharp chemical scissors for the pattering of graphene, the direct contact between graphene and photo mask introduced a high risk of damaging to graphene [9]. RIE, when used for the shaping of graphene usually begets conflict between etching rate and anisotropic profile [11]. If the etching rate increases, it causes higher concentration of reactive species inducing higher gas pressure, which ultimately creates more collision decreasing its anisotropic profile. This may cause a loss of graphene feature integrity during the etching process. In contrast, ion-milling etching, as the main preferred high throughput dry etching in semiconductor industry, have not been reported for the fabrication of graphene biosensors due to the difficulties in the removal of resulting residue in the subsequent processes [12]. In addition, for the fabrication of Cr/Au electrodes on top of graphene after its geometric shaping by ion-milling, sputtering has barely been reported due to a large amount of irremovable post-etch resist residue shell generated during ion-milling and the difficulties in lifting up the sputtered Au as sonication cannot be used due to its potential damages to graphene [13,14].

Here, we report a novel technique, which ensures not only the precise patterning of the large-scale CVD graphene on SiO_2 substrate using ion-milling, but also the complete removal of photoresist during the lift-off process for the fabrication of immunosensors without the need of using sonication which is detrimental to graphene. The novelty here is the addition of an extra thermal baking process under DUV before both ion-milling and lift-off process, which hardens the photoresist layer and avoid the difficult to remove the highly cross-linked photoresist in the subsequent processes. By using this technique, conventional thin film processing methods, such as ion-milling, sputtering and lift-off techniques, can now be used for graphene shaping and electrodes fabrication, which greatly promoted the development of graphene electronics. The resultant graphene immunosensors exhibit ultrahigh sensitivity for the label-free detection of human chorionic gonadotropin (hCG) [15,16].

2. Experimental

2.1. Reagents and apparatus

Monolayer CVD graphene was purchased from Graphene Supermarket (USA). Photoresist 1805 G2, lift-off resist 3B (LoR), the corresponding developer and remover were purchased from A-Gas Electronic Materials. All the other chemicals, such as PANSE, iron nitride, nitric acid, phosphate-buffered saline tablet (PBS), Poly (methyl methacrylate) (PMMA), etc. at biochemical grade were purchased from Sigma Aldrich (Dorset, UK). Bovine serum albumin (BSA) at biochemical grade was purchased from Sigma Aldrich (Dorset, UK). 100 μg hCG (ab126652) lyophilized powder and 1 ml of 0.02 mg/ml complementary anti-hCG (ab8466) in PBS buffer were purchased from Abcam. The prepared stockers with a concentration of 1 μg/ml were stored at −20 °C.

Electrical analysis, such as I_d-V_g and I_d-V_d measurements, was carried out at room temperature with a Keysight multi-channel source meter combined with a Cascade Microtech probe station MPS 150 under ambient conditions. Cross-section analyses of photoresist and lift-off resist were performed with scanning electron microscope (SEM) with an acceleration voltage of 10 kV. The quality of wet transferred CVD graphene was characterized by the HORIBA XPLORA Raman Spectroscopy, which is equipped with a 532 nm laser and integrated with an OLYMPUS BX41 microscope. X-ray photoelectron spectroscopy (XPS) was performed with Kratos AXISULTRA with a mono-chromated Al kα X-ray source (1486.6 eV) using an emission current of 10 mA and an anode potential of 12 kV (120 W). The ULTRA was used in fixed analyser transmission (FAT) mode, with pass energy of 80 eV for wide scans and pass energy 20 eV for high resolution scans. Cyclic Voltammetry (CV) measurements were carried out in 10 mM ferricyanide aqueous solution (1 M KCl solution was used as supporting electrolyte) at room temperature with a scan potential range from 0.8 V to −0.4 V and a scan rate of 100 mV/s.

2.2. Procedures

CVD graphene was transferred onto the surface of SiO_2 substrate following the reported wet transfer procedures [17]. The top layer of CVD graphene on Cu was spin-coated by a 500 nm PMMA layer and the bottom graphene layer was chemically removed by immersing the sample in 17% HNO_3 for 3 min. The floating graphene/PMMA was carefully picked up by a SiO_2 substrate and post-baked at 220 °C to promote a stronger graphene/substrate interaction. PMMA layer was then removed by immersing the sample into warm acetone at 60 °C for 30 min.

Graphene on SiO_2 substrate was firstly spin-coated by 200 nm LoR and followed by the post-baking at 175 °C for 5 min. Then, the sample was spin-coated by another layer of photoresist with a 400 nm thickness and followed by a standard photolithography step. Instead of using oxygen plasma for graphene shaping after the photolithography, a novel shaping method using ion-milling has been proposed and achieved in this work. The key step of using this technique is to bake the resist coated sample at 180 °C for about 1 h under a deep UV (254 nm) exposure, which could ensure a post-etch residue free graphene afterwards. This baking temperature has been optimized according to our experimental observations. When the resist is baked at 110 °C, the thermal crosslink could not occur between photoresist molecules, as 110 °C is the standard temperature for drying the solvent in photoresist. Therefore, the post-etch residue shell will still form during the subsequent ion-milling process. Whilst when it is baked at a temperature far above the parasitic flow temperature of photoresist, such as 250 or 300 °C, the resist layer quickly melt down and spread on the surface of graphene before the thermal crosslink happens, which leads to a significant loss of feature integrity (SEM images shown in Fig. S2 in Supplementary Information). Therefore, the baking temperature for this DUV photolysis process is balanced to ensure the occurrence of thermal crosslink and to avoid the significant loss of feature integrity. The discharge power and current for ion-milling were optimized to 100 mW and 30 mA respectively. And as an assistant, the 100 s etching process was split into five multi-stages with 1 min cooling between each two stages. After the ion-milling pattering of graphene, the photoresist layer could be easily removed by photoresist remover 1165 at 60 °C.

Likewise, for the deposition of Cr/Au electrodes, a thermal DUV baking was carried out before the sputtering deposition of the metal layers. Cr layer with a thickness of 2–3 nm was chosen as a non-destructive adhesion layer. 50–60 nm Au was sputtered on top of Cr as the contact material through the shield-based deposition method [18]. The base pressure and Ar pressure for sputtering deposition were 2×10^{-7} Torr and 4 mTorr respectively. Water cooling system and thermal shim applied to the back of substrate all the time were found helpful to the successful fabrication.

To provide a biologically active surface, where the anti-hCG could bond onto, PANSE has been chosen for the functionalization of graphene channel through a non-covalent method [19]. 0.0385 g PANSE powder was added into 5 ml methanol with modest shaking for 5 h to prepare 2 mM PANSE solution (if the graphene channel is fully covered by PANSE, the bio-detection later on will be limited by the minimal current difference, whilst if the concentration of PANSE is too low, the sensitivity will be limited by the number of

antibodies immobilized on graphene channel [20]). The graphene FETs were then immersed into this resulting solution and sealed tightly for 2 h at room temperature, followed by methanol rinsing to remove the non-bonded PANSE molecules from the surface of graphene. Afterwards, the functionalized graphene channels were covered by anti-hCG solution with a concentration of 100 μg/ml and incubated at room temperature for 2 h. The surface of graphene channel was rinsed with PBS buffer and immersed in BSA solution with a concentration of 0.5 mg/ml to block the free amino groups, avoiding the non-specific binding of hCG. hCG solution with different concentrations ranging from 1 pg/ml to 100 ng/ml were prepared by diluting 1 μg/ml stocker with PBS buffer and then incubated on graphene channel at room temperature for 2.5 h to ensure the strong antibody/antigen binding. The graphene FETs were rinsed by PBS buffer and DI water before any characterization.

3. Results and discussions

3.1. Ion-milling graphene shaping and electrodes sputter deposition

The qualities of graphene shaped by the normal and the novel ion-milling process have first been characterized by optical microscope. Fig. 1 (a) shows the graphene channel shaped by the normal ion-milling and lithographic process. It can be seen that the unwanted graphene has been completely etched away by exposing it to Ar ion beam; however, the photoresist and the LoR layer used for masking purpose remained after the standard chemical cleaning process (shown as cyan color in Fig. 1 (a)), which acts as an insulating layer on top of graphene, leading to the failure of FET device fabrication. To help removing this resist layer, a magnetic stirring step has been added during the lift-off process in photoresist remover. Although it has helped in the removal of resist layer to some extent (60% resist lifted off, as shown in Fig. 1 (b)), the quality of resulting graphene channel is still far away from decent for the practical fabrication of graphene electronic devices. In addition, the violent stirring of solution leads to a risk of damage to graphene. As a contrast, after graphene was shaped by the novel ion-milling and lift-off process, the resist layer on graphene channel can be completely removed, as shown in Fig. 1 (c). In this case, neither post-etch residue nor visible cracks of film can be optically seen throughout the whole channel area of the resulting device after a thorough cleaning process, indicating a good feasibility of being used in the large-scale production of graphene electronic devices, as shown in Fig. 1 (d). The graphene is located between two dashed lines and the Cr/Au electrodes are shown as white bright structures. Any adjacent two electrodes can be used as one drain and one source. The gating voltage is applied on the highly doped Si substrate (back of the substrate). A separated optical image is provided in Fig. S3 in Supplementary Information to further demonstrate the FET structure.

The qualities of graphene shaped by the normal and the novel ion-milling etching have also been characterized by Raman spectroscopy. Compared with the one taken from graphene shaped by the novel ion-milling etching, a strong band around 1540 cm^{-1} can be seen in the representative spectrum taken from the graphene channel shaped by the normal etching and lift-off methods, as shown in Fig. 1 (e), indicating the presence of a thick layer of sp^3 C-based polymer layer on top of graphene. A high resolution Raman mapping of around 1540-1580 cm^{-1} (across a graphene channel area of 35 × 35 μm in Fig. 1 (d)) has also been provided in Fig. 1 (f). The higher intensity dots showing red and yellow color are the atomic damage and defects within graphene plane, which has a similar defect density compared with that of graphene before being shaped. Expect these instinctive defects, no peaks or high intensity area can be seen around 1540 cm^{-1}, indicating the non-destructive and residue-free nature of this novel etching and lift-off technique.

3.2. Cross-section analysis of deep UV baking effect

A comparison of the cross-section profiles of photoresist-LoR bilayer with and without pre-DUV baking after ion-milling or sputter deposition is provided in Fig. 2 to explain the mechanism of this novel shaping technique. Fig. 2 (a) shows the cross-section image of ion-milled resist layer without pre-DUV baking. Both of

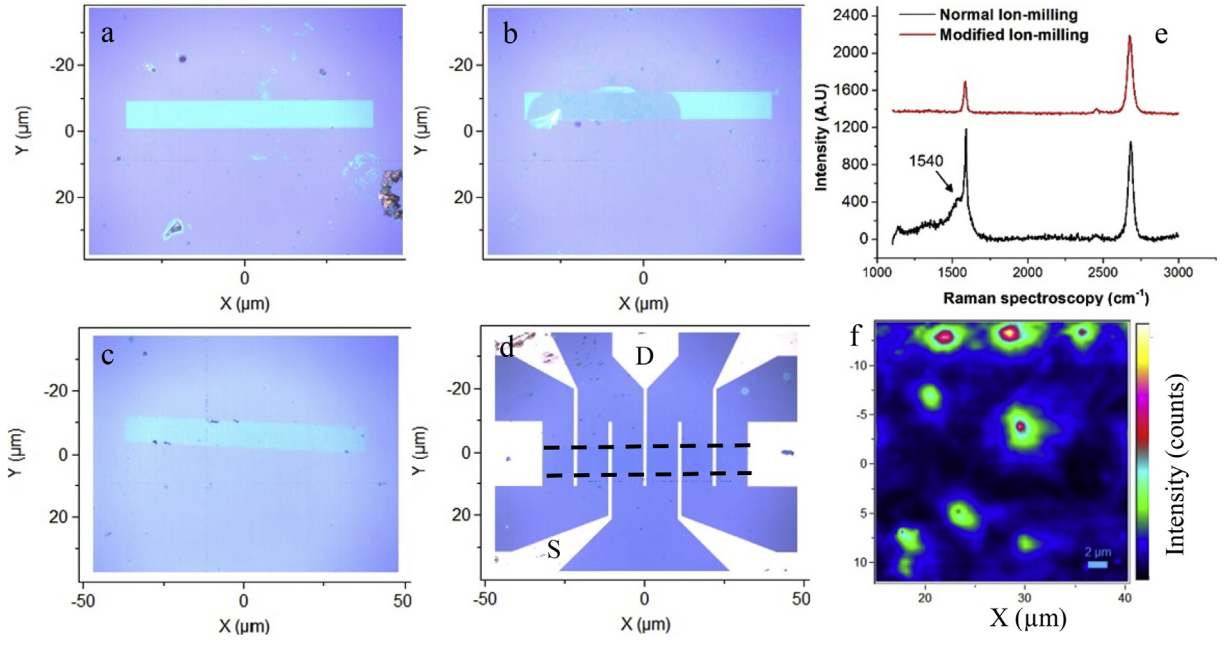

Fig. 1. Optical and Raman characterization of ion-milling shaped graphene. CVD graphene shaped by (a) normal, (b) stirring remover and (c) DUV baking ion-milling methods. (d) FET fabricated using ion-milling patterned graphene. (f) Raman mapping of D band across 35 × 35 μm area. (A colour version of this figure can be viewed online.)

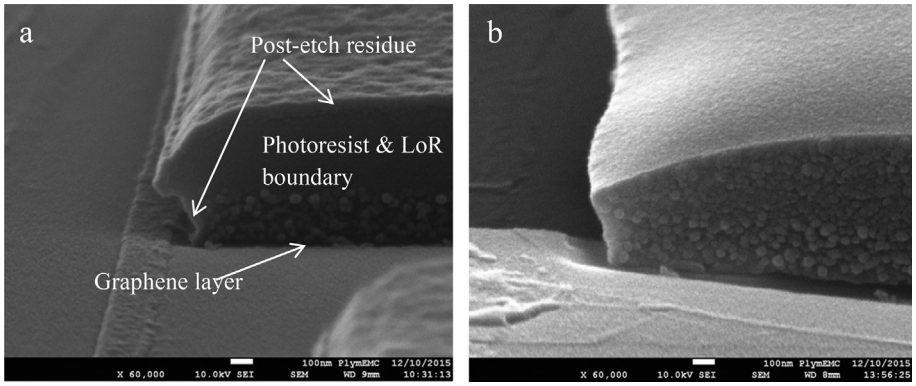

Fig. 2. Cross-section analysis of photoresist-LoR layer (a) without and (b) with DUV baking before ion-milling process, showing that the DUV hardening of the photoresist/LOR layers prevented the formation of a post-etch residue shell during ion-milling or sputter-deposition process and hence significantly improved the removability of the photoresist on graphene.

the photoresist and the LoR layer were rectangular with sharp edges after the developing process. However, it can be seen that after the ion-milling process, the edge of photoresist has got rounded and the boundary between photoresist and LoR is distinguishable, implying a melting & soften process of photoresist during the ion bombarding process. In addition, a hardened outer layer can be seen on the surface of the photoresist-LoR layer, which comes down to the surface of the SiO_2 substrate along the side walls of photoresist-LoR layer, as indicated by the arrows. As a contrast, the cross-section profile of the photoresist-LoR layer with pre-DUV baking is presented in Fig. 2 (b) (no difference can be seen from SEM images of photoresist-LoR layer before and after ion-milling process). Neither the hardened outer layer surrounding the surface of the photoresist-LoR layer nor the visible photoresist-LoR boundary can be seen in this case, indicating a thoroughly thermal cross-link process inside the resist layer before ion-milling.

The mechanism here is: the parasitic flow temperature of carbon-based photoresist S1805 G2 is about 130–135 °C. When the Ar ions are bombarding the surface of photoresist without pre-DUV baking, the local temperature could reach a few hundreds even thousands Celsius, which heats up the photoresist and leads to a thermal flow within the outer layer of the photoresist. In this case, the outer layer of the photoresist, particularly at the edges, gets melted quickly and the molecules of photoresist chemically reacted with each other at high temperature, resulting a complex stubborn polymeric layer surrounding the shaped features (also known as post-etching residues) [21] rather than simply cross-linked photoresist. This polymeric shell right through the SiO_2 substrate and links up the substrate, preventing the photoresist-LoR from coming off in the later steps [22]. In contrast, when the patterned photoresist/LOR layers have been exposed to DUV at 180 °C before the ion-milling etching or sputter-deposition, the whole photoresist layer is thermally cross-linked and hardened, which prevents the formation of post-etching residue shell at the high local temperature during the ion-milling process and hence maintain the integrity and significantly improve the removability of the photoresist without the need of using sonication which is detrimental to graphene. It is notable that this shaping and lift-off technique can be transferred and applied to the other plasma etching of graphene (such as sputtering etching) and no difference of the quality of graphene underneath can be detected by Raman.

3.3. Fabrication of hCG biosensor

A schematic illustration of the fabrication of hCG biosensor is shown in Fig. 3. The first stage of fabrication is to transfer the CVD graphene grown on top of Cu foil onto SiO_2 substrate following the wet transfer procedures. The shaping of CVD graphene channel and the deposition of Cr/Au electrodes are achieved via the novel shaping and lift-off process, which enlarges the tool choices for the fabrication of graphene electronics. Then, PANSE, which consists of a hydrophobic pyrenyl moiety base and a bio-active ester head and is used as the linker molecules between the chemically inert graphene and anti-hCG, is self-assembled onto the surface of graphene channel via π-π interaction. XPS and CV analysis of PANSE immobilization can be found in Supplementary Information. The immobilization of anti-hCG molecules onto graphene channel is achieved through a nucleophilic substitution reaction between the primary and secondary amino functionalities existing on the protein surface and the succinimidyl ester from PANSE. This nucleophilic substitution is self-activated, and therefore, no pre-treatment of antigen with EDAC/NHS chemistry is required. Based on the different amount of hCG bonded onto channel area, a difference in the electronic output will be resulted in the label-free detection.

3.4. Qualitative detection of hCG

The hCG protein and its complementary antibody were chosen as antigen-antibody pair for the feasibility verification of the label-free biosensing as it has been widely reported and used as a diagnostic marker of pregnancy and also a tumor marker for certain cancers [15,16,23]. Electrical characterization has been carried out to monitor each step of biosensor fabrication, which presents a qualitative detection of hCG protein in PBS buffer. Fig. 4 (a) shows the I_d - V_d characteristics of the plain graphene FET, the PANSE functionalized graphene FET, the anti-hCG immobilized graphene FET and the hCG bonded graphene FET. The lowest resistance with a value of 10.5 kΩ can be seen from the plain graphene FET (black). After the graphene was modified with PANSE linker, the resistance almost doubled to 22 kΩ (red). After the anti-hCG was immobilized onto the surface of graphene, the resistance increased to 33.6 kΩ. With the specific binding of hCG protein onto its antibody, the resistance further increased to 72 kΩ. This phenomenon is attributed to the structural change of graphene channel in electronic devices: each carbon atom in the honeycomb structured graphene lattice posses a free electron, which forms the electron cloud on both sides of graphene with electrons from other carbon atoms, leading to a low resistivity in the electronic measurement [24]. After the immobilization of PANSE linkers via π-π stacking, the electron cloud is disturbed by this insulating material, which is in accordance with Fig. 4 (b), leading to an increased resistance. With the addition of anti-hCG and hCG onto the graphene channel, these

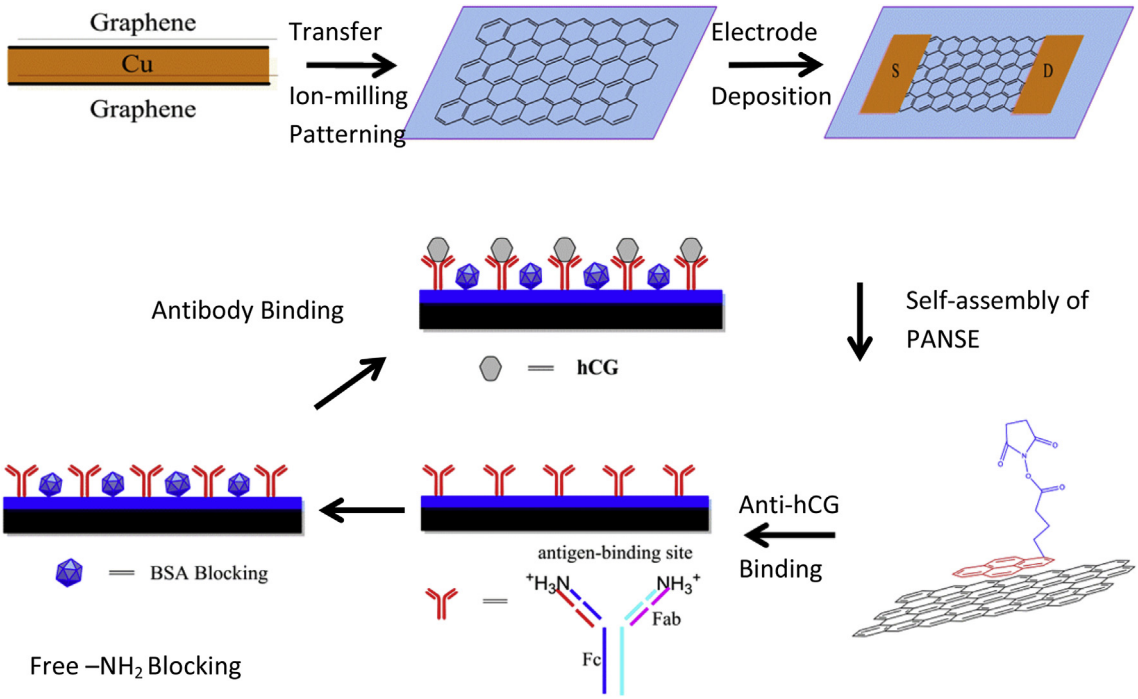

Fig. 3. Schematic illustration of hCG biosensor fabrication. (A colour version of this figure can be viewed online.)

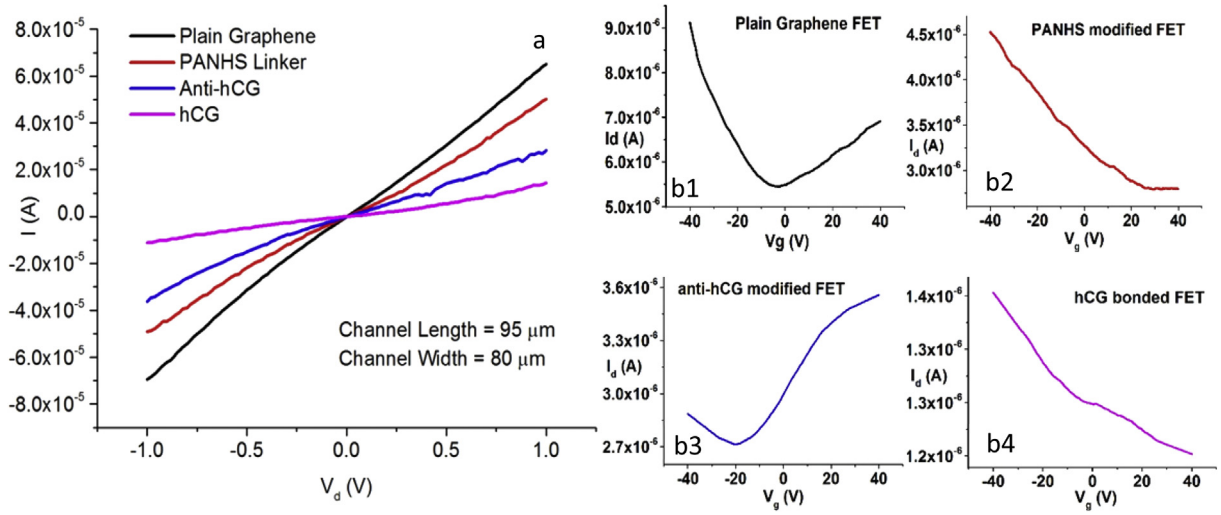

Fig. 4. Qualitative label-free detection of hCG protein in PBS buffer. (a) I_d-V_d and (b) I_d-V_g characteristics of plain graphene FET, PANSE novel FET, anti-hCG novel FET and FET after hCG bonded onto it (the concentration of hCG in PBS is μg/ml). (A colour version of this figure can be viewed online.)

protein molecules chemically bonded with the linker and antibody, which results in a further increased resistance due to the insulting nature of protein. The corresponding I_d - V_g characteristics of each step in Fig. 4 (a) have also been provided and shown in Fig. 4 (b1) - (b4). The Dirac point of the plain graphene FET has been found around −2 V at the beginning, which confirm the effectiveness of our novel residue-free shaping technique. Then the Dirac point positively shifted to 30 V after adding PANSE, confirming the successful modification and p-type performance of PANSE. With the addition of anti-hCG and hCG, the Dirac point shifted to −20 V and then back to +40 V (beyond instrument limit), which not only presents a qualitative detection for hCG in PBS buffer but also illustrates the infeasibility of using Dirac point as indicator for qualitative detection of higher hCG concentration. Therefore, the I_d-V_d characterization is chosen for the later work quantitative detection of hCG in PBS.

3.5. Dependence of hCG concentration and electric resistance

In order to validate the sensing response, the quantitative detection of hCG is achieved by analyzing the changes of the electric resistance. For all surface modification steps, such as linker attachment, antibody immobilization, BSA blocking and detection of hCG protein, similar conditions of modification was attempted except the differential concentration of hCG protein. This facilitates similar output in all modifications but a difference in resistance

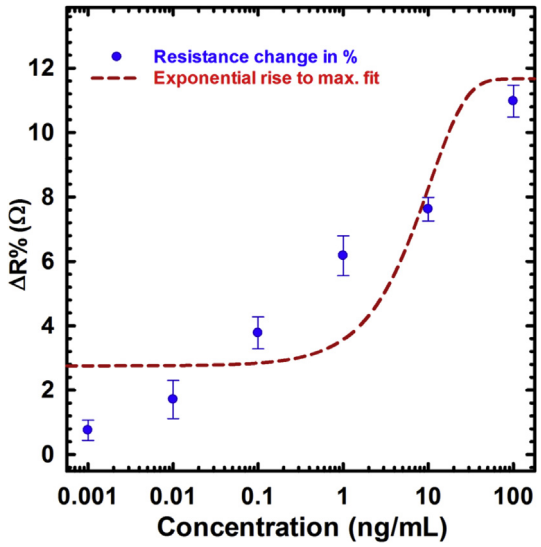

Fig. 5. The measured resistance change in % after blocking agent deposition versus concentration (in logarithmic scale). The red dotted line corresponds to the fitting results by using a lognormal function $y = y_0 + a\,(1\text{-}e^{-bx})$, with $y_0 = 2.27$, $a = 24.79$. (A colour version of this figure can be viewed online.)

from BSA blocking to antigen detection.

The results of resistance changes from BSA blocking to the detection of different hCG concentration ranging from 1 pg/ml up to 100 ng/ml is shown in Fig. 5. The result represents the plot of average resistance change versus the log of the concentration of hCG binding signal. This plot is fit to a Three Parameter Single Exponential Rise to Maximum function, which includes data points with error bars representing the standard deviation. From this plot we were able to obtain the LOD based on the three fold of standard deviation the lowest concentration and the slope of the calibration curve to be 6 pg/ml. Note that the exponential rise to maximum fit though looks saturated from 1 pg/ml to 1 ng/ml, it's a logarithmic scale. The lower standard deviation error for 10 pg/ml is almost at the parallel to the highest point of the error bar of 1 pg/ml. This points out that the LOD would be lower or around 10 pg/ml. In addition the biosensor clearly shows that no pre- or post-amplification process is required to monitor anti-hCG and hCG interaction as low as 6 pg/ml. The baselines for concentration dependent test on back-gated FET sensors are at the point to blocking agent deposition on the graphene surface. Hence, the typical negative controls with PBS or DI water are not taken into consideration. Thus, this ultrahigh sensitivity towards the detection of hCG protein proofs the effectiveness of our novel technique in the removal of resist residues. Also, this ultralow limit of detection is 10^3 time of the hCG concentration in 3rd week of pregnancy's urine, which leads to an application in the industrial biosensor production [25]. Moreover, being the back-gated FET, it would not require additional electrical devices to process the signal like that of optical or electrochemical devices, which leads to easiness of application in the industrial biosensor production. At present, the sensor is for one-time use for only one analyte only. To add more value to the devices for practical reusable applications with higher selectivity and stability, further work on this sensing method is currently underway.

4. Conclusions

A novel technique for the shaping of graphene channels and fabrication of back-gated graphene FET immunosensors has been developed by employing a DUV hardening process prior to the ion-milling of graphene channels or sputter-deposition of Au electrode layers. The quality of resulting graphene FET biosensors was confirmed by Raman spectroscopy, optical spectroscopy and the label-free detection of an ultralow concentration of human chorionic gonadotropin. We approved that the photoresist layer is thermally cross-linked and hardened after the deep UV treatment of the patterned photoresist/LOR layers before the ion-milling etching or sputter-deposition. This novel technique prevents the post-etching residue shell formed at the high local temperature during the ion-milling etching or sputtering deposition of electrodes, hence, maintain the integrity and significantly improve the removability of the photoresist without the need of using sonication. The novel shaping technique provides a cost-effective and large-scale production compatible process for fabricating graphene biosensors. The ion-milling shaped graphene immunosensors exhibit a wide linear range and a high sensitivity for the label-free hCG detection.

Notes

The authors declare no competing financial interest.

Acknowledgment

We acknowledge the financial support from the UK EPSRC under grand NO. EP/M006301/1, China Scholarship Council and the technical support on XPS from National EPSRC XPS Users' Service (Newcastle University).

Appendix A. Supplementary data

Supplementary data related to this article can be found at http://dx.doi.org/10.1016/j.carbon.2017.03.032.

References

[1] B. Li, G. Pan, S.A. Awan, N. Avent, Techniques for production of large area graphene for electronic and sensor device applications, Graphene 2D Mater. 1 (2014) 2299–3134.
[2] K.S. Novoselov, D. Jiang, F. Schedin, T.J. Booth, V.V. Khotkevich, S.V. Morozov, et al., Two-dimensional atomic crystals, P. Natl. Acad. Sci. U. S. A. 102 (2005) 10451–10453.
[3] J. Tian, P.-X. Yuan, D. Shan, S.-N. Ding, G.-Y. Zhang, X.-J. Zhang, Biosensing platform based on graphene oxide via self-assembly induced by synergic interactions, Anal. Biochem. 460 (2014) 16–21.
[4] N. Mohanty, V. Berry, Graphene-based single-bacterium resolution biodevice and DNA transistor: interfacing graphene derivatives with nanoscale and microscale biocomponents, Nano Lett. 8 (2008) 4469–4476.
[5] K.I. Bolotin, K. Sikes, Z. Jiang, M. Klima, G. Fudenberg, J. Hone, et al., Ultrahigh electron mobility in suspended graphene, Solid State Commun. 146 (2008) 351–355.
[6] X. Lu, H. Huang, N. Nemchuk, R.S. Ruoff, Patterning of highly oriented pyrolytic graphite by oxygen plasma etching, Appl. Phys. Lett. 75 (1999) 193–195.
[7] J. Li, T.-F. Chung, Y.P. Chen, G.J. Cheng, Nanoscale strainability of graphene by laser shock-induced three-dimensional shaping, Nano Lett. 12 (2012) 4577–4583.
[8] D.C. Bell, M.C. Lemme, L.A. Stern, J.R. Williams, C.M. Marcus, Precision cutting and patterning of graphene with helium ions, Nanotechnology 20 (2009) 455301–455306.
[9] L. Zhang, S. Diao, Y. Nie, K. Yan, N. Liu, B. Dai, et al., Photocatalytic patterning and modification of graphene, J. Am. Chem. Soc. 133 (2011) 2706–2713.
[10] B.S. Archanjo, A.P.M. Barboza, B.R.A. Neves, L.M. Malard, E.H.M. Ferreira, J.C. Brant, et al., The use of a Ga + focused ion beam to modify graphene for device applications,", Nanotechnology 23 (2012) 255305–255311.
[11] D. Choi, C. Kuru, C. Choi, K. Noh, S.-K. Hong, S. Das, et al., Nanopatterned graphene field effect transistor fabricated using block Co-polymer lithography, Mater. Res. Lett. 2 (2014) 131–139.
[12] S. Myneni, D.W. Hess, Post-plasma-etch residue removal using CO 2-based fluids, J. Electrochem. Soc. 150 (2003) G744–G750.
[13] X. Zhang, J.Q. Pham, H.J. Martinez, P.J. Wolf, P.F. Green, K.P. Johnston, Water-in-carbon dioxide microemulsions for removing post-etch residues from patterned porous low-k dielectrics, J. Vac. Sci. Technol. B 21 (2003)

2590–2598.
[14] Q. Le, M. Claes, T. Conard, E. Kesters, M. Lux, G. Vereecke, Removal of post-etch photoresist and sidewall residues using organic solvent and additive combined with physical forces, Microelectron. Eng. 86 (2009) 181–185.
[15] U.-H. Stenman, H. Alfthan, K. Hotakainen, Human chorionic gonadotropin in cancer, Clin. Biochem. 37 (2004) 549–561.
[16] H. Lund, K. Løvsletten, E. Paus, T.G. Halvorsen, L.O. Reubsaet, Immuno–MS based targeted proteomics: highly specific, sensitive, and reproducible human chorionic gonadotropin determination for clinical diagnostics and doping analysis, Anal. Chem. 84 (2012) 7926–7932.
[17] Q. Yu, J. Lian, S. Siriponglert, H. Li, Y.P. Chen, S.-S. Pei, Graphene segregated on Ni surfaces and transferred to insulators, Appl. Phys. Lett. 93 (2008), 1131031–1-113103-3.
[18] B. Li, G. Pan, N.Y. Jamil, L. Al Taan, S. Awan, N. Avent, Shielding technique for deposition of Au electrical contacts on graphene by sputtering, J. Vac. Sci. Technol. A 33 (2015), 030601–1-030601-5.
[19] F. Liu, Y.H. Kim, D.S. Cheon, T.S. Seo, Micropatterned reduced graphene oxide based field-effect transistor for real-time virus detection, Sens. Actuator. B Chem. 186 (2013) 252–257.
[20] F. Liu, K.S. Choi, T.J. Park, S.Y. Lee, T.S. Seo, Graphene-based electrochemical biosensor for pathogenic virus detection, BioChip J. 5 (2011) 123–128.
[21] D. Beery, K. Reinhardt, P.B. Smith, J. Kelley, A. Sivasothy, Post etch residue removal: novel dry clean technology using densified fluid cleaning (DFC), in: Interconnect Technology, 1999. IEEE Int. Conference, 1999, pp. 140–142.
[22] S. De Gendt, J. Wauters, M. Heyns, A novel resist and post-etch residue removal process using ozonated chemistry,", Solid State Technol. 41 (1998) 57–60.
[23] B. Li, G. Pan, N.D. Avent, R.B. Lowry, T.E. Madgett, P.L. Waines, Graphene electrode modified with electrochemically reduced graphene oxide for label-free DNA detection, Biosens. Bioelectron. 72 (2015) 313–319.
[24] S. Chen, L. Brown, M. Levendorf, W. Cai, S.-Y. Ju, J. Edgeworth, et al., Oxidation resistance of graphene-coated Cu and Cu/Ni alloy, ACS Nano 5 (2011) 1321–1327.
[25] S. Teixeira, N.S. Ferreira, R.S. Conlan, O. Guy, M.G.F. Sales, Chitosan/AuNPs modified graphene electrochemical sensor for label-free human chorionic gonadotropin detection, J. Electroanal. 26 (2014) 2591–2598.